ISBN: 978-3-95450-204-2 ISSN: 2673-5350 doi:10.18429/JACoW-IBIC2019-MOBO04

CHARACTERIZATION AND FIRST BEAM LOSS DETECTION WITH ONE ESS-nBLM SYSTEM DETECTOR

L. Segui*, H. Alves, S. Aune, J. Beltramelli, Q. Bertrand, M. Combet, A. Dano-Daguze, D. Desforge, F. Gougnaud, T. Joannem, M. Kebbiri, C. Lahonde-Hamdoun, P. Le Bourlout, P. Legou, O. Maillard, A. Marcel, Y. Mariette, J. Marroncle, V. Nadot, T. Papaevangelou, G. Tsiledakis,
IRFU-CEA, Université Paris-Saclay, F-91191, Gif-sur-Yvette, France
I. Dolenc Kittelmann, T. J. Shea, European Spallation Source ERIC, Lund, Sweden

Abstract

The monitoring of losses is crucial in any accelerator. In the new high intensity hadron facilities even low energy beam can damage or activate the materials so the detection of small losses in this region is very important. A new type of neutron beam loss monitor has been developed specifically targeting this region, where only neutrons and photons can be produced and where typical Beam Loss Monitors (BLM), based on charged particle detection, could not be appropriate because of the photon background due to the RF cavities. The BLM proposed is based on gaseous Micromegas detectors, designed to be sensitive to fast neutrons and with little sensitivity to photons. Development of the detectors presented here has been done to fulfil the requirements of ESS and they will be part of the ESS-BI systems. The detector has been presented in previous editions of the conference. Here we focus on the neutron/gamma rejection with the final FEE and in the first operation of one of the modules in a beam during the commissioning of LINAC4 (CERN) with the detection of provoked losses and their clear separation from RF gammas. The ESS-nBLM system is presented in this conference in a separate contribution.

INTRODUCTION

A new type of beam loss monitor (BLM) based on the detection of fast neutrons have been conceived, constructed and characterized. Moreover, the response of a pre-series detector to beam losses and RF gammas background has been tested at Linac4, at CERN. Such detector has been developed in the context of an in-kind contribution from CEA-Saclay to ESS, constituting one of the ESS Beam Instrumentation (ESS BI) systems, namely the neutron sensitive BLM (nBLM) system [1].

The proposed detector aims to extend the sensitivity in the low energy region of an hadron accelerator. In such region only gammas and neutrons can be used as beam losses signature. The goal is to detect the produced fast neutrons while having a low sensitivity to gammas that are also produced by the RF cavities. Moreover, the detector will exhibit low sensitivity to thermal neutrons which will have lost their location information due to their moderation and they can be also produced by the surroundings.

Two complementary types have been proposed, both based on Micromegas detectors as readout. The project started in July 2016 and in the last two years, after the conceptual design phase, the detectors have been characterized at different irradiation facilities. In the following section the geometry and operation of the modules will be explained in detail. Afterwards, experimental results showing discrimination of neutrons from gammas will be presented. Finally, the first beam loss detection at LINAC4 (CERN) will be shown, as proof of detector capabilities.

* laura.segui@cea.fr

DETECTOR CONCEPT AND DESIGN

The nBLM proposed is based on Micromegas readout [2]. They are gaseous amplification structures part of the MPGD family (Micro-Pattern Gaseous Detectors), successors of the wire chambers, with high gain, fast signals, and a very good spatial and energy resolution.

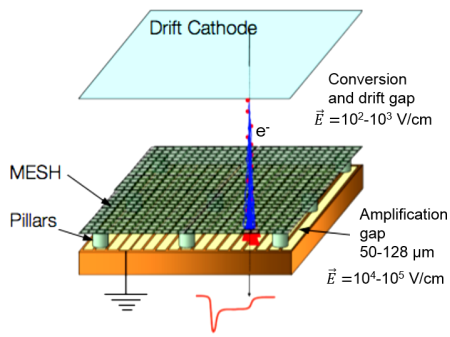

Figure 1: Sketch of Micromegas detector operation.

Micromegas devices operate with two regions separated by a micromesh: the conversion region and the amplification region (see Fig. 1). The detector itself consists on a mesh suspended over an anode by insulator pillars, usually made by litographic process [3,4]. It operates always with a third parallel plate as cathode. The conversion region is defined between the cathode and the mesh, and is where the primary electrons are produced when a charged particle ionizes the gas (usually an electric field of ~100 V/cm–1000 V/cm is applied). The amplification region is defined between the mesh and the anode and is where an avalanche of electrons is produced that will induce a detectable signal in both the mesh and the anode. In this region the electric field is much higher, usually of ~1×10^4 V/cm–1×10^5 V/cm to produce the avalanche. The amplification gap is usually of 50 µm–125 µm while the conversion distance varies according to the application. The anode can be made by strips or pixels as well.

ISBN: 978-3-95450-204-2 ISSN: 2673-5350 doi:10.18429/JACoW-IBIC2019-MOB004

To detect the neutrons, they have first to be converted into charged particles (unless we are interested in the signals produced by neutron recoils). One possibility is to place a solid converter layer at the entrance of the conversion region, in the cathode.

nBLM Detectors Geometry

Two kinds of modules have been conceived, main difference being the neutron-to-charged particle conversion, while the gas chamber and the Micromegas are identical in both cases. We will refer to them in the following as fast and slow module based on the type of losses they were designed for. In the fast detector, the proton recoils produced by a collision of neutrons into mylar (125 µm for operation at ESS) is what ionizes the gas. The proton will be emitted with an energy that depends on the initial neutron energy and incidence angle giving in general a continuous proton energy spectrum. Only if the initial neutron energy is larger than 0.5 MeV the proton will have enough energy to escape the material making the detector intrinsically blind to slow and thermal neutrons. Aluminized mylar is used to give voltage to the cathode easily.

In the case of the slow detector, the conversion is done in a solid layer of few µm of $^{10}B_4C$ deposited on the cathode[1] (aluminium plate). A $^{10}B(n,\alpha)^7Li$ reaction will take place and the alpha will have enough energy to escape the layer of boron and to ionize the gas (~1.4 MeV). To increase its efficiency the gas chamber is surrounded by 5 cm of polyethylene that moderates the fast neutrons before interacting with the boron layer. To make the detector blind to thermal neutrons an external layer of absorber, made by 5 mm of borated rubber from Mirrotron company [5], is used. A sketch of both modules is shown in Fig. 2. The geometry has been optimized for the ESS accelerator, but different parameters can be easily changed to adapt to the expected flux in different facilities.

The detectors are bulk Micromegas [3] equipped with the fast front-end electronics cards (FEE) placed on-board of the Micromegas, outside the gas volume, and protected by a Faraday cage. The FEE is based on the FAMMAS current amplifiers (Fast Amplifier Module for Micromegas ApplicationS) [6], amplyfing the signal before transmitting it to the DAQ system. Most of the measurements have been done with a drift distance of 1.7 mm–1.8 mm.

DETECTOR PERFORMANCE

During the conceptual phase of the design, Monte Carlo simulations were carried out to optimize the geometry. Initial studies were done in FLUKA [7] and continued in Geant4 [8] and shown in [9]. For almost each irradiation test, Geant4 simulations have been also performed. Main results of the characterization were shown in last year IBIC conference [10]. Of special relevance are the results regarding gamma/neutron discrimination.

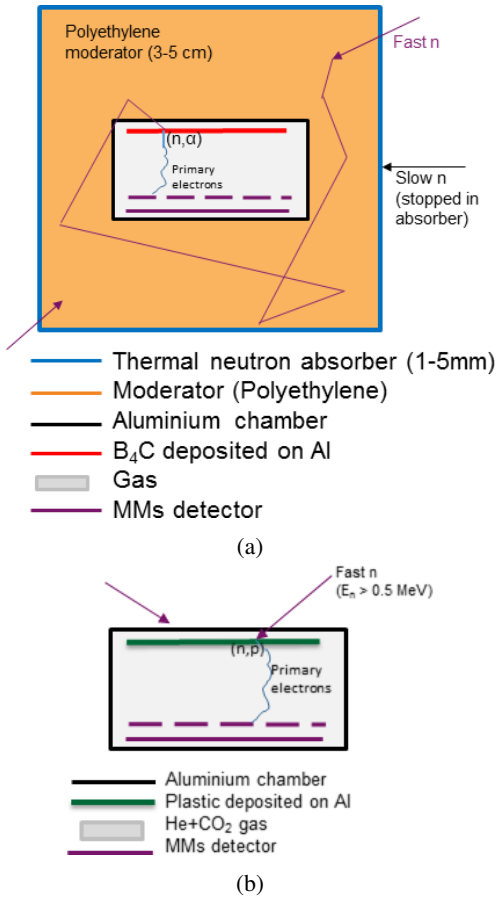

Figure 2: Neutron detection principle of the slow module (a) and of the fast one (b). More details can be found in the text.

First confirmation of the separation between neutrons and gammas was obtained in measurements in a monoenergetic neutron facility at IRSN Cadarache as shown in [10]. In that case, when calibrating the detectors using a 565 keV neutron field, gammas of 6 MeV–7 MeV were also produced. The contribution of gammas was estimated by replacing the LiF target by AlF where only gammas are produced. Comparison of the efficiencies measured with both targets can then be used to determine the gamma contribution in case of LiF target. Gammas will create charge along their path by Compton scattering due to the short drift distance producing an exponential decay deposit energy spectrum. In the case of the slow detector the alphas produced by the neutrons will deposit an almost constant energy well separated from the exponential with an appropriate gain. However, in the fast detector, the protons produced by the neutrons are emitted with different energies and the deposited spectrum will overlap much more with the gammas one. Data acquired in Cadarache was a good indication for the slow module of the gamma/neutron separation, however, for the fast one, the dependency of the discrimination with the applied energy

[1] The deposition was made by the ESS Detector Coatings Workshop in Linköping, Sweden. The thickness of the coating for the data shown here and the baseline of operation at ESS is 1.5 µm.

ISBN: 978-3-95450-204-2 ISSN: 2673-5350 doi:10.18429/JACoW-IBIC2019-MOBO04

threshold is larger and varies case by case as the proton energy depends on the neutron energy. Moreover, data was acquired with a charge amplifier and shaper and not with the final electronics. Therefore, data with the final detector and using the final FEE card were collected with a neutron source (AmBe 10^{11} Bq, neutrons up to 10 MeV) and with a gamma source (^{60}Co, ~8×10^{10} Bq, gammas at 1.17 and 1.33 MeV) in collaboration with the CEA-Saclay Radioprotection Service (SPR). Measurements were taken at different gains and drift voltages to determine the best operational point (mesh voltages studied from 440 to 525 V). The gammas were only detectable with a voltage above 480 V while neutrons are detectable much before.

Data were recorded using a high sampling rate Teledyne LeCroy oscilloscope at 250 Ms/s recording the full waveforms in frames of 1 µs. With a C++ based on ROOT [11] code each recorded event that exceeds a given threshold (2.5 mV in this case) is analysed and its main pulse characteristics (amplitude, charge, pulse duration, …) identified. In Fig. 3 we see the amplitude distribution for neutrons (black) and gammas (red) for the two modules (Fig. 3a for the slow detector and Fig. 3b for the fast). The spectra have been normalized by the measurement time and by the activity of each source at the surface of the detector (around 2×10^6 Bq for the neutrons and 2×10^{10} Bq for the gammas). In both cases, the gamma distribution fits well to an exponential (as already observed in previous measurements [10]) as they create charge along their path by Compton scattering without depositing all their energy, due to the short drift distance for such gamma energies. The events that are in the gamma run at higher energies are due, indeed, to neutrons coming from the neutron source stocked not far away from the place of measurements as can be seen in the background run (see Fig. 4). In the case of the slow detector, the cut-off observed at around 10 mV is due to the auto-trigger in the scope. We can see how most of the signals due to neutrons can be well separated from the gammas in the slow detector. In the case of the fast detector the neutron amplitude spectrum overlaps much more with the gammas (see Fig. 3b) as protons are emitted with an initial energy that depends on the initial neutron energy, as mentioned before. However, they can arrive to energies well above the gamma limit, making the rejection possible at the expense of neutron efficiency. Note that the gamma distribution was only measured with the slow module however we do not expect to have any difference between modules. To study the dependency of the discrimination between both populations with the amplitude threshold, the relative efficiency with respect to it has been calculated for each case. Results are shown only for the case with V_m = 500 V and V_d = 750 V, an operational point we found optimal. In the case of gamma spectrum, the exponential fit is used to calculate the efficiency to reduce the background contamination. Results for this particular case are shown in Fig. 5. We observe that, in the case of the slow, the neutron efficiency remains more or less constant for all amplitude thresholds, over the scanned threshold range, arriving to negligible gamma sensitivities. In the fast, as

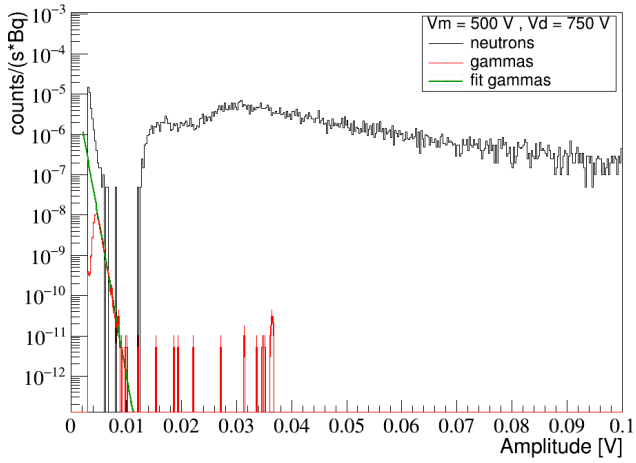

(a)

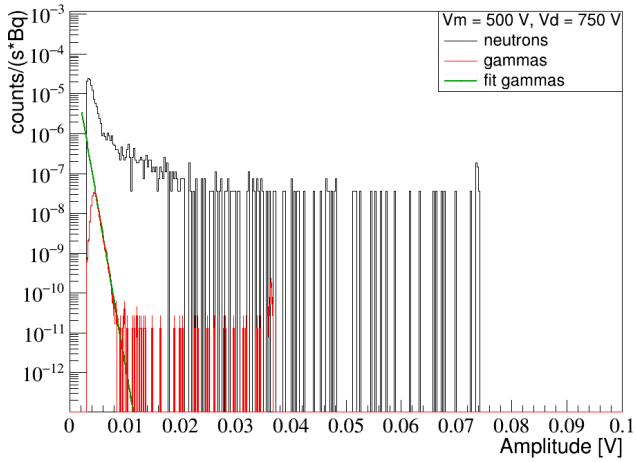

(b)

Figure 3: Amplitude distribution of neutrons (black) and gammas (red) for each detector: a) for the slow and b) for the fast. Exponential function has been fitted to the distribution for gammas. It determines quite correctly the best amplitude threshold to discriminate the gammas to a negligible value. Measurements were done at the "baseline" operational point for ESS V_{mesh} = 500 V, and V_{drift} = 750 V.

expected, the neutron efficiency is highly affected. If we use the limit of the exponential fit (~ 10 mV) as an indication we have a rejection of gammas of ~ 2×10^{-6} while the neutron efficiency remains the same in the slow detector and decreases about an order of magnitude for the fast detector. In next section we will see how in real accelerator conditions this is not a limitation to detect beam losses produced by neutrons over the gamma background from the RF.

BEAM LOSS DETECTION AT LINAC4

In August 2018 one fast module was installed at LINAC4 (CERN) to take data during its commissioning. Two data campaigns have been carried out since then. In the first one (November 2018) the detector response was investigated, gammas from RF were detected and we saw the power of rejection between neutrons produced by the beam and gammas

ISBN: 978-3-95450-204-2 ISSN: 2673-5350 doi:10.18429/JACoW-IBIC2019-MOBO04

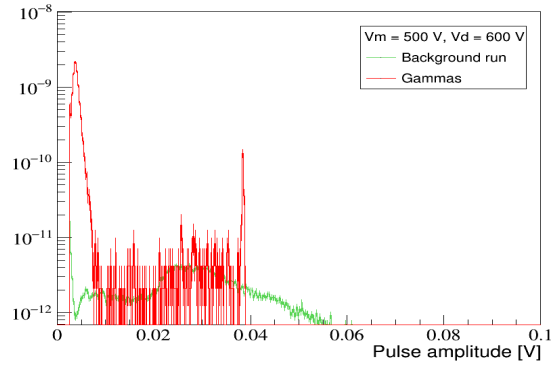

Figure 4: Amplitude spectrum obtained with the slow detector with a gamma source (red) compared to a background run (green). The high amplitude events that are seen in both cases correspond to neutrons coming from the neutron source used also in the measurements and that was stocked not far away.

from the RF. In the second campaign (December 2018) beam losses were provoked in the machine and clearly identified by the nBLM module. Data were recorded as explained in previous section, using a high sampling rate oscilloscope, and same pulse analysis applied. In this case data were recorded either triggering with the LINAC4 trigger, or in auto-trigger mode but recording the trigger information to correlate *a posteriori* the events with the machine time. The analysis to identify pulses is the same and the rate is calculated for a LINAC4 machine cycle of 1.2 µs using the difference in time between events. Data were acquired in long window frames (few milliseconds) to reduce any dead time effect from the recording of the oscilloscope. Data was also acquired with the acquisition that will be used in the ESS-nBLM system based on the IOxOS IFC_1410 AMC equipped with one IOxOS ADC_3111 FMC board. Results are also shown in this conference in [1].

In the first campaign the accelerator was operating in normal conditions. We had to operate the detector at high gain to start detecting signals (V_{mesh} = 550 V with a drift voltage of V_{drift} = 1650 V) which were of very small amplitude, as can be seen in Fig. 6a, except from time to time when some higher amplitude event was observed. A long run in auto-trigger mode was taken in those field conditions who help to understand that in fact those small pulses were distributed along the RF pulse (~ 750 µs, as is observed in Fig. 6a) and corresponded to gammas from the RF. This observation was later confirmed with the data taken in December with much more statistics shown in the following.

In the second campaign (December 2018), beam losses were provoked uniformly along the accelerator. Measurements were done at different gains in the nBLM module and runs were taken when the machine was operating normally and when losses were provoked. We will use the longer run, taken over one night, and where losses were produced during only 10 minutes, to illustrate how the identification of gammas from RF and neutrons from the beam is done. The

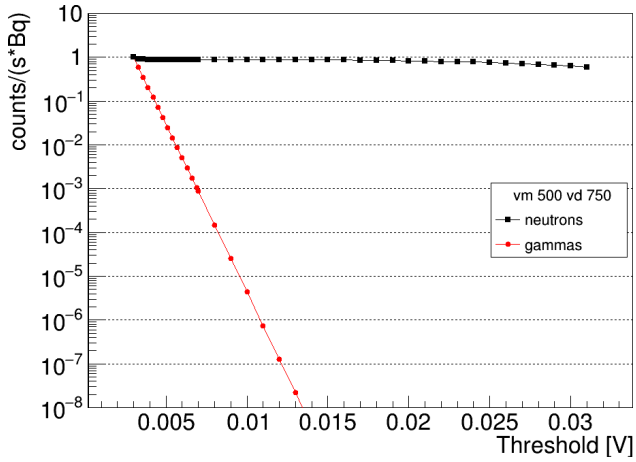

(a)

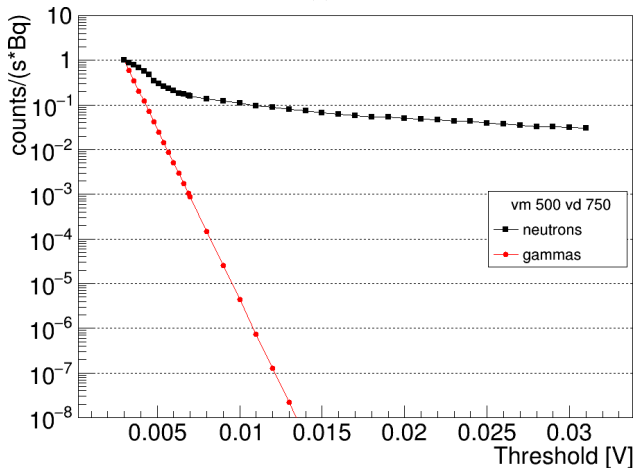

(b)

Figure 5: Relative efficiencies with respect to different amplitude thresholds for neutrons (black) and gammas (red) for each detector (a) slow and (b) fast. Measurements were done at the "baseline" operational point for ESS V_{mesh} = 500 V and V_{drift} = 750 V.

conditions of this run are very similar to the ones in November 2018 (V_{mesh} = 550 V and V_{drift} = 1500 V). Observing the time distribution of the events (Fig. 7b in black for all events that exceed the "noise" threshold, set at 2.5 mV), we can see how they are mostly homogeneously distributed along ~ 850 µs which, for this particular run, corresponds to the RF pulse. Note that data was taken during the commissioning of the machine where the conditions were varying. We see also some events later corresponding probably to noise events. In the first part of the distribution we observe an excess of events in a time window of about 150 µs. If we observe now the amplitude distribution (Fig. 7a black for all events that exceed the "noise" threshold) we observe an exponential distribution at lower amplitudes with a tail at higher amplitudes. The exponential part is very similar to what we have measured and shown in previous section for gammas. Indeed, if we apply different amplitude cuts (different colors in Figs. 7a and 7b) we observe how the temporal

ISBN: 978-3-95450-204-2 ISSN: 2673-5350 doi:10.18429/JACoW-IBIC2019-MOB004

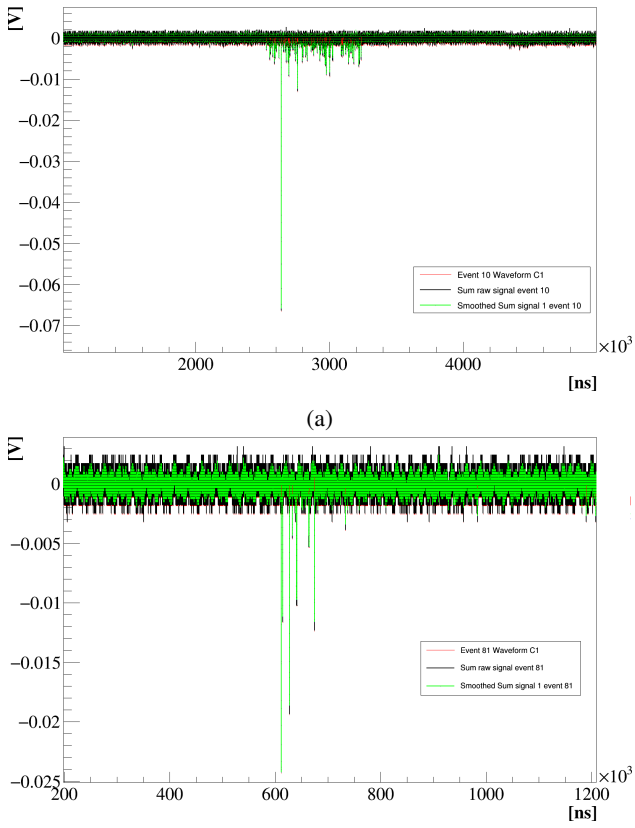

Figure 6: In this figure we show the events taken at LINAC4 as recorded with the oscilloscope (black) and once smoothed (green). Each pulse corresponds to a single particle. In (a) we can see an example for a case of normal operation, where we detect mainly the gammas from RF (small amplitude) and distributed along the RF pulse (750 µs in this case). In this particular frame one neutron was also detected. In (b) we can compare with a provoked loss case where mainly high amplitude events (neutrons) were detected and distributed along the beam pulse duration (150 μs). Note that we had to operate the detector at high gains (V_{mesh} = 550 V) to start detecting high amplitude events. The drift voltage was set to V_{drift} = 1650 V in (a) and to V_{drift} = 1500 V in (b).

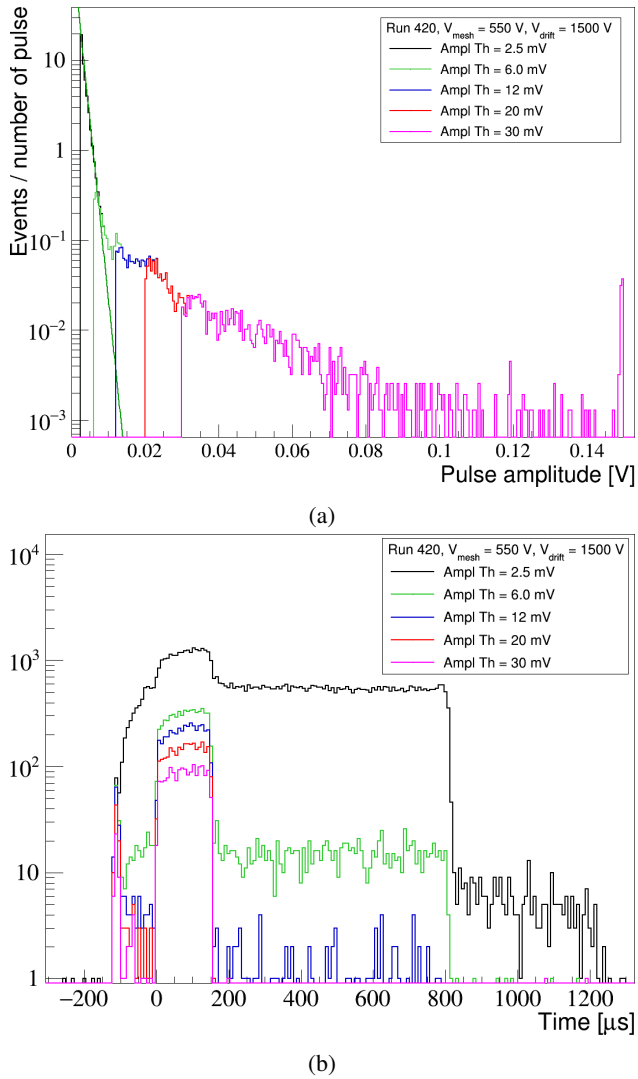

Figure 7: (a) Amplitude distribution measured with the nBLM fast module installed at LINAC4 in one long run (11 hours) taken in December 2018 in which a beam loss was provoked for 10 minutes and the rest was operating in normal conditions. In black corresponding to all events that exceed the noise threshold set at 2.5 mV, and in colors for different amplitude thresholds. (b) Time distribution of the detected events for same different energy thresholds. We can see how the distribution narrows from ~ 850 µs to 150 µs when applying an amplitude cut, times corresponding respectively to the RF pulse and beam pulse durations proving how the small amplitude events who, indeed, fit to the exponential, are distributed along the RF pulse and correspond to x-rays or gammas events coming from it.

distribution of the events narrows until it has the duration of the LINAC4 beam of 150 µs during this run, although some events are also observed in the first 100 µs. After discussion with the LINAC4 experts those times seem to correspond to the conditions of the machine for this particular run (both for the RF duration and beam pulse duration). Further discussions and analysis are on-going but results are also consistent with the data acquired with the FMC acquisition card and shown in [1]. The potential to discriminate the RF gammas with either the detector gain (at lower V_{mesh} the gammas were indistinguishable from the noise) or with an energy threshold, as shown in previous section, is clearly proven.

The amplitude spectrum measured for runs with or without losses have been compared for two dfferent gains. They are shown in Fig. 8 (red with losses and black with no losses) with the voltages being V_{mesh} = 525 V and V_{drift} = 1000 V in Fig. 8a and V_{mesh} = 550 V, V_{drift} = 1500 V (as before) in Fig. 8b. When losses occurred the high energy region of the spectrum started to be populated in both cases while the exponential due to gammas ends still at the same point. Observing the end point of the exponential fit, a neutron energy threshold of 6 mV or 20 mV is chosen for each gain and the

ISBN: 978-3-95450-204-2 ISSN: 2673-5350 doi:10.18429/JACoW-IBIC2019-MOB004

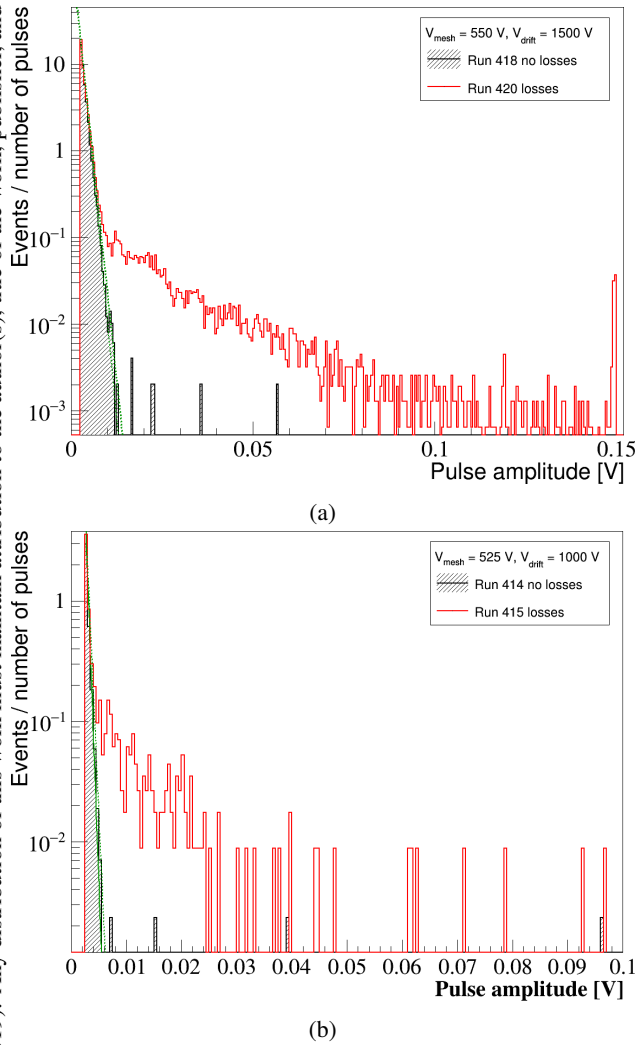

Figure 8: Amplitude distribution for runs where a loss is produced (in red) and runs without losses (in black) compared between them for two different gains: in (a) for V_{mesh} = 550 V,V_{drift} = 1500 V and in (b) V_{mesh} = 525 V, V_{drift} = 1000 V). In both cases the amplitude spectrum starts to detect higher amplitude events due to the produced neutrons in the loss. Those neutrons will create protons in the neutron-to-charge-particles converter in the detector that ionize more the gas than the produced charge by the gammas from the RF that arrive to it. The dashed-green lines in all cases are the fits of the first part of the spectra to an exponential that is due to the RF gammas. We observe how these lines are the same in the case with or without losses and its end-point can be use to set the threshold to have a clean neutron selection for each operation conditions.

rate of neutrons is computed for both cases (run with/without losses) obtaining a clear difference between both cases of at least a factor 100 between the run with losses and no losses (depends on the voltage). It is interesting to mention that for the no losses cases the same rate was obtained. In Fig. 8a the runs were short, of about five minutes in same conditions all the time (loss/no loss). For run 420, corresponding to the long run left overnight and discussed before, a loss was provoked at 20:50 for about ten minutes, as is clearly identified in the measured rate shown in Fig. 9. The rest of the time the rate is stable and about 450 times smaller. Although this was an off-line analysis, the idea behind it is very similar to the neutron detection logic which constitute a part of the real-time FPGA-based data processing in the ESS nBLM system [1, 12] and proves the capability of the nBLM detector to identify losses and to discriminate them from the gammas produced by the RF cavities.

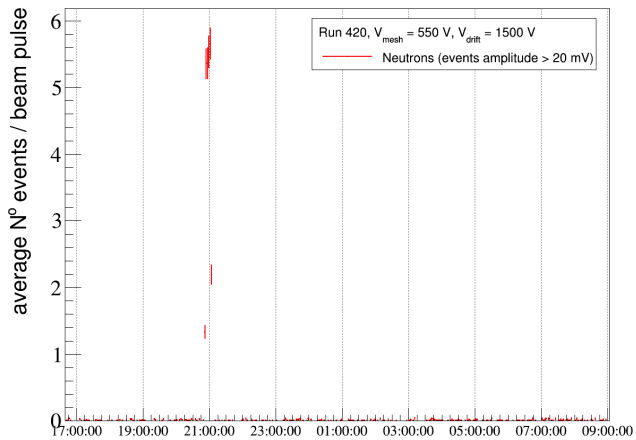

Figure 9: Neutron rate along time as measured with the fast nBLM detector installed at LINAC4 (CERN). A clear increase is observed at 20:50, time when losses were produced in the machine for about 10 minutes. The neutron rate was calculated with the events that exceed a neutron selection cut of 20 mV.

CONCLUSION

A new type of Beam Loss Monitor, based on the detection of the fast neutrons produced by the protons hitting accelerator parts, using gaseous Micromegas detectors have been developed. The ESS-nBLM system is composed by two complementary module types and will be part of the ESS-BI systems. It is dedicated mainly to the DTL region (low energy part) where mainly neutrons and photons are produced by beam losses. The detector have been characterized in several data campaigns to confirm their expected functionality before delivery to ESS.

One of the advantages with respect to other BLM is the strong discrimination capability between neutrons and gammas on a pulse by pulse basis, due to their differences in ionization power of different particles. The identification of neutrons originated by beam losses over RF background events have been proven testing a prototype at LINAC4.

The installation of the first detector at ESS is planned for the coming months and the commissioning is expected with the first beam.

ACKNOWLEDGEMENTS

The authors would like to thank R. Hall-Wilton, C. Höglund and L. Robinson from the ESS Detector Coatings

ISBN: 978-3-95450-204-2 ISSN: 2673-5350 doi:10.18429/JACoW-IBIC2019-MOBO04

Workshop in Linköping, Sweden for the fabrication and production of the boron converter. The authors will also like to thank J. Krai, W. Vigano and C. Zamantzas for making possible the tests at LINAC4. Thanks also to M. Guelin and G. Aatz for the use of the CEA SPR installations and radioactive sources. L. Segui would like to acknowledge the financial support of Enhanced Eurotalents program (an FP7 Marie Skłodowska-Curie COFUND program). The project was supported by the French in-kind contribution to ESS AIK-7.9 and the H2020 project AIDA-2020, GA no.654168.

REFERENCES

[1] I. Dolenc Kittelmann *et al.*, "Neutron sensitive Beam Loss Monitoring System for the ESS Linac", presented at the 8th Int. Beam Instrumentation Conf. (IBIC'19), Malmö, Sweden, Sep. 2019, paper MOPP022, this conference.

[2] I. Giomataris, P. Rebourgeard, J.P. Robert, and G. Charpak, "MICROMEGAS: a high-granularity position-sensitive gaseous detector for high particle-flux environments", *Nucl. Instr. Meth. A*, vol. 376, p. 29, 1996.

[3] I. Giomataris *et al.*, "Micromegas in a bulk", *Nucl. Instr. Meth. A*, vol. 560, pp. 405–408, 2006.

[4] Andriamonje, S. *et al.*, "Development and performance of Microbulk Micromegas detectors", *Journal of Instrumentation*, vol. 5, no. 02, p. P02001, 2010.

[5] Mirrotron Ltd, https://mirrotron.com/en

[6] P. Legou *et al.*, "Beam Spectrometers using Micromegas in Time Projection Chamber mode" in *Proc. HB'06*, Tsukuba, Japan, 2006, paper WEBZ03, p. 256.

[7] T.T. Böhlen, F. Cerutti, M.P.W. Chin, A. Fassò, A. Ferrari, P.G. Ortega, A. Mairani, P.R. Sala, G. Smirnov and V. Vlachoudis, "The FLUKA Code: Developments and Challenges for High Energy and Medical Applications", *Nuclear Data Sheets*, vol. 120, pp. 211-214, 2014.
A. Ferrari, P.R. Sala, A. Fasso, and J. Ranft, "FLUKA: a multi-particle transport code", CERN-2005-10 (2005), INFN/TC_05/11, SLAC-R-773.

[8] GEANT Collaboration, S. Agostinelli *et al.*, "GEANT4 a simulation toolkit", *Nucl. Instr. Meth. A*, vol. 506, pp. 250–303, 2003.

[9] J. Marroncle *et al.*, "A New Beam Loss Monitor Concept Based on Fast Neutron Detection and Very Low Photon Sensitivity", in *Proc. 5th Int. Beam Instrumentation Conf. (IBIC'16)*, Barcelona, Spain, Sep. 2016, paper TUAL02, pp. 278–282.

[10] L. Segui *et al.*,, "A Micromegas Based Neutron Detector for the ESS Beam Loss Monitoring" in *Proc. 7th International Beam Instrumentation Conference (IBIC'18)*, Shanghai, China, September 2018, paper TUPA02, p. 211–214.

[11] Rene Brun and Fons Rademakers, "ROOT - An Object Oriented Data Analysis Framework" in *Proceedings AIHENP'96 Workshop*, Lausanne, September 1996, *Nucl. Inst. & Meth. in Phys. Res. A*, vol. 389, pp. 81–86, 1997. See also http://root.cern.ch/.

[12] G. Jabłonski *et al.*, "FPGA-based Data Processing in the Neutron-Sensitive Beam Loss Monitoring System for the ESS Linac", in *MIXDES 2019*, Rzeszów, Poland, June 2019, pp. 101–105. doi:10.23919/MIXDES.2019.8787166